HHS Public Access

Piezoresistor-Embedded Multifunctional Magnetic Microactuators for Implantable Self-Clearing Catheter

Qi Yang [Student Member, IEEE],

Department of Electrical and Computer Engineering, Purdue University, West Lafayette, IN 47907 USA

Albert Lee,

Goodman Campbell Brain and Spine, Department of Neurological Surgery, Indiana University, Indianapolis, IN 46202 USA

R. Timothy Bentley,

College of Veterinary Medicine, Purdue University, West Lafayette, IN, 47907 USA

Hyowon Lee [Member, IEEE]

Weldon School of Biomedical Engineering, Birck Nanotechnology Center, Purdue University, West Lafayette, IN 47907 USA.

Abstract

Indwelling catheters are used widely in medicine to treat various chronic medical conditions. However, chronic implantation of catheters often leads to a premature failure due to biofilm accumulation. Previously we reported on the development of a self-clearing catheter by integrating polymer-based microscale magnetic actuators. The microactuator provides an active anti-biofouling mechanism to disrupt and remove adsorbed biofilm on demand using an externally applied stimulus. During an *in vivo* evaluation of self-clearing catheter, we realized that it is important to periodically monitor the performance of implanted microactuators. Here we integrate gold-based piezoresistive strain-gauge on our magnetic microactuators to directly monitor the device deflection with good sensitivity (0.035%/Deg) and linear range (±30°). With the integrated strain-gauge, we demonstrate the multi-functional capabilities of our magnetic microactuators that enable device alignment, flow-rate measurement, and obstruction detection and removal towards the development of chronically implantable self-clearing smart catheter.

Keywords

Piezoresistive sensor; strain gauge; magnetic microactuators; biofouling; implantable device

I   Introduction

Indwelling catheters are one of the most widely used medical devices for the treatment and the management of various chronic cardiovascular, intravascular, neurological, and urological disorders [1]–[3]. Specialized catheters such as central venous access device and insulin infusion sets are also used often to continuously deliver various life-saving drugs for cancer and diabetes patients [4]. However, many indwelling catheters have limited lifetime

due to biofouling and thrombosis-related failure [1], [5]. For example, 14-18% of central venous catheters experience catheter-related thrombosis that can lead to pulmonary embolism, infection, and loss of catheter function [6]. Similarly, chronically implantable shunt systems used for treatment of hydrocephalus have a 30-day shunt failure rate of up to 23-26%, which necessitates numerous revision surgeries for these patients [7].

To combat the biofouling-related failures in chronically implanted catheters, we have previously reported on the development of self-clearing catheters using thin-film polymer-based magnetic microactuators [8]–[11]. The application of magnetic field from a remote source causes a large out-of-plane deflection for these microdevices. When a time-varying magnetic field is used, the microactuator delivers forceful vibration inside the catheter to break apart and remove adsorbed biofilm. The polyimide-based microactuator is robust enough for large actuation cycles (>300 million) and is rugged enough to withstand up to 7-Tesla MRI [10], [12]. However, during our preliminary *in vivo* evaluation on the efficaciousness of the self-clearing catheter, the need to periodically monitor the mechanical responses of the microactuators became apparent. We learned that, once implanted, it is impossible to verify whether the device is oriented properly or even actuating as expected. Moreover, we realized that it is difficult to determine whether the animal condition is deteriorating due to a failed device or other complications.

Several groups proposed novel impedance-based sensors to monitor catheter obstruction [13], [14]. Similar impedance-based sensing may be used to determine whether the microactuator cleared the catheter obstruction. However, monitoring the catheter patency alone does not provide a direct evidence of microactuator movement. Therefore, we needed a method to measure the amplitude of device deflection to help determine the efficacy of microactuation *in situ*. In this work, we integrated piezoresistive strain sensors on our actuators to directly monitor the device movement. The strain gauge is fabricated on our existing magnetic microactuator without significant modification to the existing process flow.

The piezoresistive effect refers to the change in a material's resistivity due to an applied mechanical strain [15]. For microscale strain sensing, semiconductor materials are typically chosen for their high gauge factor ($G = \frac{\Delta R}{R\epsilon}$), which relates the change in resistance R with the baseline resistance R and the applied strain ϵ. For example, a single crystal silicon is known to have $G > 150$ and doped diamond film have $G > 2000$ [16], [17]. However, most semiconductor-based piezoresistors require a high temperature processing ($> 400°$) for deposition and annealing, which is not compatible with our flexible polymer substrate. Although metallic piezoresistors have much lower G (~1) than semiconductor or nanoscale materials [18], [19], they can provide adequate sensitivity to generate detectable signal given the relatively large deflection of our magnetic microactuators. Moreover, there are several examples of using noble metal piezoresistors for implantable microdevices for their biocompatibility and linearity [20], [21].

Here we demonstrate gold (Au) piezoresistor-integrated magnetic microactuators with good sensitivity (0.035%/Deg) and linear range (±30°). These multifunctional microactuator now provide additional capabilities including device alignment, flow rate measurement, and

obstruction detection on top of the existing self-clearing feature. The added functionalities enabled by the piezoresistor represents the next step towards our ultimate goal of creating a chronically implantable smart catheter that can self-diagnose its status and clear any obstructions without additional surgery.

II. Device Design and Fabrication

A. Device Design

The general structure of the flexible micro magnetic actuator mirrors our previous design [10]. The device consists of a rectangular polyimide flexure with a tip mass structure attached at the end. The tip mass structure consists of a near circular polyimide base and a Ni ferromagnetic element on top, which rotates in response to the applied magnetic field and deflects the flexure. The Au piezoresistor is located at the base of the flexure to maximize the change in resistance. The shape of piezoresistor follows a simple serpentine pattern to maximize the net resistance given the confined space [22]. The design has three windings evenly distributed at the width of the cantilever. The entire area of piezoresistor including the contact pads has a total of 109 effective squares in which 94% is on the region that experiences the most stress during the device deflection.

B. Microfabrication Process

The process flow of our first-generation polymer-based magnetic microactuators was modified to fabricate the strain-gauge embedded version [10]. Fig. 1 illustrates the fabrication steps. On top of a 100-mm single-side polished silicon wafer, a 500-nm of silicon dioxide (SiO_2) release layer was deposited using PECVD (Axic, Milpitas, CA). Next, polyimide (PI2525, HD Microsystem, Parlin, NJ) was spin coated at 1600 rpm and cured in a nitrogen oven. Prior to coating, an adhesion promoter (VM-652, HD Microsystem, Parlin, NJ) was applied on the oxide layer to improve adhesion. The polyimide thickness was verified to be 10.7μm using an Alpha-Step IQ surface profiler (KLA-Tencor, Milpitas, CA).

Next, the piezoresistor (20 nm Cr and 50 nm Au) was deposited on top of polyimide layer using an e-beam evaporator (Airco) and patterned using lift-off. Following the metal deposition, a second layer of polyimide was spin-coated at 8000 rpm to achieve 1.2 μm-thickness. The Cr/Au adhesion and conduction layers were then evaporated on the wafer globally in preparation for Nickel (Ni) electroplating. A 8-μm-thick of Ni ferromagnetic element was deposited and defined by the plating mold (AZ9260, MicroChemicals GmbH, Ulm, Germany). Afterwards, the outline of structural plate, cantilever and device boundary were dry-etched using oxygen (O_2) plasma (Advanced Oxide Etcher, STS, Newport, UK). Polyimide pattern was etched down until the sacrificial SiO_2 layer was exposed. The samples were released in 6:1 buffered oxide etchant that removed the sacrificial layer. After the devices were detached and collected, the piezoresistor contact pads were opened up using an O_2 plasma.

C. Device Integration into Catheters

The integration of the thin-film device into an implantable catheter requires a good alignment between the actuator and the inlet pore. Once integrated, the thin-film device

needs to be immobilized to withstand the continuously flowing fluid. Furthermore, an electrical connection between the piezoresistor and test equipment needs to be established. To satisfy these requirements, a 'needle and thread' integration approach was developed. Two 15-inch long magnet wires were aligned and attached to the gold contact pads located at the end of the piezoresistor. Electrically conductive joints between wires and pads were formed by applying liquid silver paste (CI-1001, Engineered Conductive Materials, Inc, Delaware, OH) and curing on hotplate at 85 °C for 10 min. The wires along with actuator substrate were then transferred and bonded to a small piece of polyimide tape for increased structural integrity. Afterwards, the entire sample was coated with Parylene C (PDS2010, Specialty Coating System, Indianapolis, IN) to improve electrical insulation and biocompatibility.

Next, the microactuator substrate was cut so that it can fit inside the lumen of the catheter. Using a commercial implantable catheter (Central Venous Catheter Set, Cook Inc. Bloomington, IN), a 1.2-mm-diameter pore was manually punched. The free ends of the two wires were inserted through the pore and pulled out from the catheter opening. The actuator was then dragged through the pore opening to complete the assembly. Once the thin-film device entered the lumen of the catheter, it curled around the inner wall. Finally, the catheter end with wires was sealed with silicone adhesive. To test the robustness of the integration, deionized water (DI) was manually injected to catheter opening using a 10 ml syringe. The actuator was able to withstand five consecutive bursts of flow (>5 ml/s) without being dislodged or shifting in position. Fig. 1 shows an example of fully assembled smart catheter with piezoresistor-embedded multifunctional magnetic microactuator.

III.   Device Characterization and Results

A.   Static and Dynamic Responses

A bespoke electromagnet and a test fixture were used to assess the performance of the piezoresistive strain gauge in a fully integrated smart catheter. The fundamental function of the strain gauge is to provide static deflection angle as a function of percentage resistance change. The change in resistance was measured through the wired connection using a custom LabVIEW program (2013, National Instruments, Austin, TX) in a 4-wire resistance measurement mode. A static deflection response was measured by actuating the device in short magnetic pulses at different magnetic flux density (10–50 mT) produced by the electromagnet in a direction perpendicular to the catheter pore (Fig 2). Static deflection results showed that the thin-film piezoresistors has adequate sensitivity (0.035%/Deg) with a range −30° to 30°. The expected percentage change in resistance R was calculated by equating the cantilever deflection angle φ to maximum stress σ_{max} produced by a point force F on the tip of cantilever:

$$\phi = \frac{FL^2}{2EI}; \sigma_{max} = \frac{FLt}{2I};   \quad (1)$$

$$\frac{\Delta R}{R} = G\frac{\sigma_{max}}{E} = \frac{Gt\phi}{L} \quad (2)$$

with cantilever beam length L, thickness t, elastic modulus $E = 2.45$GPa for polyimide, and the moment of inertia $I = \frac{wt^3}{12}$ for rectangular beam. Experimental results indicated that our Au piezoresistor has $G = 1.1$, which corresponds well with values from literatures (Fig. 2).

The dynamic response of the magnetic actuator also was characterized using the integrated strain gauge. A sinusoidal magnetic field(<10 mT) was swept from 5 Hz to 1 kHz in 20 s using our custom electromagnet. The resistance was sampled at 6.48 kHz and the amplitude spectrum representing the relative deflection was converted into the frequency response using Fourier transform. Fig. 3 shows the dynamic responses of a cantilever in air and in deionized water. The results indicated that our integrated strain gauge can detect critical dynamic characteristic of our magnetic actuators (i.e, resonant frequencies and quality factors).

B. In Situ Device Alignment and Positioning

Minimizing the misalignment between the direction of applied magnetic field relative to the position of the implanted device is critical to maximizing the device deflection. However, it is difficult to ascertain whether the device is fully deflecting once it is implanted. Even with live fluoroscopic imaging, the microscale device is too small to resolve visually. The integrated strain gauge is able to provide a method to optimize the device alignment with the external magnetic field and to determine whether the device is actually deflecting.

The relationship between misalignment angle θ and cantilever deflection φ can be described by balancing the mechanical (τ_{mech}) and the magnetic torque (τ_{mag}):

$$\tau_{mech} - \tau_{mag} = 0 \quad (3)$$

$$k_\phi - v_m MH \sin\left(\frac{\pi}{2} - \theta - \phi\right) = 0 \quad (4)$$

with the rotational stiffness $k_\phi = \frac{EI}{L}$, the volume of magnet v_m, the magnetization $M = 0.6T$ for Nickel, and the applied magnetic field strength H. For a given magnetic field strength H, the deflection angle φ can be solved as a function of misalignment angle θ. The cantilever displacement will be smaller with greater misalignment.

Experimentally, this relation was measured using the integrated strain gauge. At the center of our electromagnet, a fully integrated smart catheter was taped at the bottom of a beaker supported by a custom 3D printed test fixture that can tilt. The text fixture was designed to

be fixed at various misalignment angles (0–50°) with respect to the horizon (Fig. 4a). The beaker was filled with DI water to mimic the bodily fluid. For each alignment angle, a magnetic field strength of 20 kA/m was pulsed for 3 s. The change in resistance was recorded using a custom LabVIEW DAQ system. Using the previously characterized strain gauge calibration, the net deflection of our actuators were estimated (Fig. 4b). With this alignment information, the orientation of external magnetic coil could be adjusted to produce the maximum deflection. In practice, clinicians may be able to utilize this information during the implantation and the actuation to optimize the placement of device and the electromagnet.

C. Flow Rate Measurement

Microactuator can not only be deflected using the externally applied magnetic field but also be deflected passively due to the bodily fluid flow. When the excess fluid is being drained through the catheter pores, the drag force can bend the cantilever inward and the resistance change can be estimated by modeling the fluid drag $F = \frac{1}{2}\rho v^2 C_d A$ on a perpendicular thin plate, with the fluid density ρ, the fluid velocity v, the drag coefficient of the plate C_d, and the area of structural plate A. The stress at base of cantilever can be derived from assuming a point force is concentrated at tip. The resistance change can then be described as

$$\Delta R = \frac{\rho v^2 C_d ARGLt}{4EI} \quad (5)$$

Bench-top experiments were performed to characterize the flow rate-resistance relationship. In an evaporating dish, a smart catheter with integrated microactuator was immobilized and submerged in DI water. The open end of the catheter was connected to a S16 tubbing (Masterflex, Cole-palmer) driven by peristaltic pump, which pumped DI water into the catheter as shown in Fig. 5a. The volume flow rate was calibrated by measuring the mass of the pumped water. The pump was driven at various flow rates (2–15 ml/min with 1ml/min decrement) and the corresponding resistance change relative to the baseline values were measured (Fig. 5). The change in resistance matched the Eq. 5 well, which suggests a good flow sensing capability for the tested range.

D. Obstruction Detection and Removal

One of the biggest clinical challenges for chronic use of indwelling catheter is non-invasively determining whether the implanted device is failing due to obstruction. By monitoring the dynamic responses of our strain-gauge embedded magnetic microactuators, it is also possible to detect the presence of an obstruction at the inlet pore of the implanted device *in situ*. To demonstrate, the baseline dynamic responses of the sample device was first measured (Fig. 6). Next, a blood clot was made using blood sample from an euthanized pig by dropping 2 ml of blood into 0.1 M phosphate buffer solution (PBS, pH 7, Fisher Scientific, Waltham, MA). The blood clot mass was then gently squeezed into the catheter pore to mimic a robust obstruction. The dynamic response of the device measured again. With the blood clot obstructing the movement, the dynamic response was suppressed

significantly (Fig. 6e). Next, a low frequency high amplitude actuation was applied (20 Hz at 25 kA/m) for 3 min, which dislodged and removed the blood clot mass. Finally, the dynamic response was then captured again to demonstrate restoration of characteristic peaks. This results illustrate the possibility of using our multifunctional microactuator to not only remove catheter obstruction but to detect the presence of the obstruction without the need for explanation.

IV. Discussions and Conclusions

Here we designed, fabricated, and tested flexible magnetic microactuators with integrated piezoresistive strain gauges to improve the functionality of chronically implantable catheters. We demonstrated that the integrated strain gauge may be used for a number of different purposes. By monitoring the resistance change as a function of microactuator deflection, we determined whether the catheter pores were aligned to provide maximum deflection. The resistance changed linearly with respect to the deflection range of $\pm 30°$, which corresponded well with the expected values. We also demonstrated the fluid flow sensing capability which may be used to monitor the CSF flow rate *in situ*. Moreover, our strain-gauge integrated microactuators showed the capability to detect the presence of catheter pore obstruction.

The additional feature enabled by integrating the strain gauge on our actuator may eventually be useful in clinical practice. However, additional work is necessary to fully embrace the integrated strain-gauge approach. Since the goal of magnetic microactuators are to prolong the lifetime of the implantable catheter, the long term reliability and sensitivity of the piezoresistive strain gauge sensor cannot be overlooked.

The resistance baseline drift is a well-recognized issue in piezoresistor-based strain gauges due to temperature fluctuation, material degradation, and mechanical fatigue [23]–[27]. Some of our devices also demonstrated increased baseline resistance over time (Fig. 5). The cause of this baseline drift is most likely due the deformation of Au contact pads. The flexible polymer substrate makes the contact pads susceptible to bend due to flow-induced shear [24]. This may be addressed by using a more secure integration method to reduce substrate deformation. The issue of resistance drift is minimized when using a pulsed (e.g., alignment) or sinusoidal actuation (e.g., fault detection) to measure the relative change in resistance [26] However, for a passive flow rate measurement, the resistance drift may be a problem since an absolute resistance value is needed. Another potential solution may be to incorporate a fixed strain gauge for a differential measurement to eliminate substrate deformation induced drift.

Our future works include improving the sensitivity of the strain gauge for a wider range of applications (i.e., urinary, neurological, and cardiac) [28]–[30]. Moreover, we plan to better characterize the long-term stability and mechanical integrity of the thin-film piezoresistor. Finally, we will incorporate a wireless capability to measure the changes in resistance for the device to be truly useful in clinical settings.

Acknowledgment

References

[1]. Sousa C, Henriques M, and Oliveira R, "Mini-review: Antimicrobial central venous catheters– recent advances and strategies." Biofouling, vol. 27, no. 6, pp. 609–620, 2011. [PubMed: 21718230]

[2]. Kestle JRW, "CSF shunts 50 years on past, present and future," Child's Nervous System, vol. 16, no. 10–11, pp. 800–804, 2000.

[3]. Haddad NJ, Cleef SV, and Agarwal AK, "Central Venous Catheters in Dialysis : The Good, the Bad and the Ugly," The Open Urology & Nephrology Journal, vol. 5, pp. 12–18, 2012.

[4]. Heinemann L and Krinelke L, "Insulin Infusion Set: The Achilles Heel of Continuous Subcutaneous Insulin Infusion," Journal of Diabetes Science and Technology J Diabetes Sci Technol, vol. 66, no. 44, pp. 954–964, 2012.

[5]. Riva-cambrin J, Kestle JRW, Holubkov R, Butler J, Kulkarni AV, Drake J, Whitehead WE, Iii JCW, Shannon CN, Tamber MS, L. DD Jr, Rozzelle C, Browd SR, Simon TD, and Clinical H, "Risk factors for shunt malfunction in pediatric hydrocephalus: a multicenter prospective cohort study," Journal of Neurosurgery: Pediatrics, no. 4, pp. 382–390, 2016.

[6]. Kamphuisen P and Lee A, "Catheter-related thrombosis: lifeline or a pain in the neck?" Hematology, pp. 638–644, 2012. [PubMed: 23233646]

[7]. Anderson IA, Saukila LF, Robins JMW, Akhunbay-Fudge CY, Goodden JR, Tyagi AK, Phillips N, and Chumas PD, "Factors associated with 30-day ventriculoperitoneal shunt failure in pediatric and adult patients," Journal of Neurosurgery, vol. Preprint, pp. 1–9, 2018.

[8]. Lee SA, Lee H, Pinney JR, Khialeeva E, Bergsneider M, and Judy JW, "Development of microfabricated magnetic actuators for removing cellular occlusion," Journal of Micromechanics and Microengineering, vol. 21, no. 5, p. 054006, 2011.

[9]. Lee H, Kolahi K, Bergsneider M, and Judy JW, "Mechanical evaluation of unobstructing magnetic microactuators for implantable ventricular catheters," Journal of Microelectromechanical Systems, vol. 23, no. 4, pp. 795–802, 2014. [PubMed: 29151776]

[10]. Yang Q, Park H, Nguyen TN, Rhoads JF, Lee A, Bentley RT, Judy JW, and Lee H, "Anti-biofouling implantable catheter using thin-film magnetic microactuators," Sensors and Actuators, B: Chemical, vol. 273, no. 6, pp. 1694–1704, 2018.

[11]. Park H, Raffiee AH, John SWM, Ardekani AM, and Lee H, "Towards Smart Self-Clearing Glaucoma Drainage Device," Microsystems & Nanoengineering, vol. ACCEPTED, 2018.

[12]. Lee H, Xu Q, Shellock FG, Bergsneider M, and Judy JW, "Evaluation of magnetic resonance imaging issues for implantable microfabricated magnetic actuators," Biomedical Microdevices, vol. 16, no. 1, pp. 153–161, 2014. [PubMed: 24077662]

[13]. Basati S, Tangen K, HSU Y, Lin H, Frim D, and Linninger A, "Impedance Changes Indicate Proximal Ventriculoperitoneal Shunt Obstruction In-vitro." IEEE Transactions on Biomedical Engineering, vol. 9294, no. c, 7 2014.

[14]. Kim BJ, Jin W, Baldwin A, Yu L, Christian E, Krieger MD, Mccomb JG, and Meng E, "Parylene MEMS patency sensor for assessment of hydrocephalus shunt obstruction," Biomedical Microdevices, pp. 1–13, 2016. [PubMed: 26660457]

[15]. Stassi S, Cauda V, Canavese G, and Pirri CF, "Flexible tactile sensing based on piezoresistive composites: A review," Sensors, vol. 14, no. 3, pp. 5296–5332, 2014. [PubMed: 24638126]

[16]. Mason W and Thurston R, "Use of piezoresistive materials in the measurement of displacement, force, and torque," The Journal of the Acoustical Society of America, vol. 29, no. 10, pp. 1096–1101, 1957.

[17]. Sahli S and Aslam D, "Ultra-high sensitivity intra-grain poly-diamond piezoresistors," Sensors and Actuators A: Physical, vol. 71, no. 3, pp. 193–197, 1998.

[18]. Lee S, Reuveny A, Reeder J, Lee S, Jin H, Liu Q, Yokota T, Sekitani T, Isoyama T, Abe Y, Suo Z, and Someya T, "A transparent bending-insensitive pressure sensor," Nature Nanotechnology, vol. 11, pp. 472–478, 2016.

[19]. Stampfer C, Jungen A, Linderman R, Obergfell D, Roth S, and Hierold C, "Nano-electromechanical displacement sensing based on single-walled carbon nanotubes," Nano letters, vol. 6, no. 7, pp. 1449–1453, 2006. [PubMed: 16834427]

[20]. Lee K-K, He J, Singh A, Massia S, Ehteshami G, Kim B, and Raupp G, "Polyimide-based intracortical neural implant with improved structural stiffness," Journal of Micromechanics and Microengineering, vol. 14, no. 1, pp. 32–37, 2004.

[21]. Chen P-J, Rodger DC, Saati S, Humayun MS, and Tai Y-C, "Microfabricated implantable parylene-based wireless passive intraocular pressure sensors," Journal of Microelectromechanical Systems, vol. 17, no. 6, pp. 1342–1351, 2008.

[22]. Wang Y-H, Lee C-Y, and Chiang C-M, "A mems-based air flow sensor with a free-standing micro-cantilever structure," Sensors, vol. 7, no. 10, pp. 2389–2401, 2007. [PubMed: 28903233]

[23]. Aiyar AR, Song C, Kim S-H, and Allen MG, "An all-polymer airflow sensor using a piezoresistive composite elastomer," Smart Materials and Structures, vol. 18, no. 11, p. 115002, 2009.

[24]. Cong P, Young DJ, Hoit B, and Ko WH, "Novel long-term implantable blood pressure monitoring system with reduced baseline drift," in Engineering in Medicine and Biology Society, 2006. EMBS'06. 28th Annual International Conference of the IEEE IEEE, 2006, pp. 1854–1857.

[25]. Ziaie B and Najafi K, "An implantable microsystem for tonometric blood pressure measurement," Biomedical Microdevices, vol. 3, no. 4, pp. 285–292, 2001.

[26]. Song C, Aiyar A, Kim S-H, and Allen M, "Exploitation of aeroelastic effects for drift reduction, in an all-polymer air flow sensor," Sensors and Actuators A: Physical, vol. 165, no. 1, pp. 66–72, 2011.

[27]. Yu L, Kim BJ, and Meng E, "Chronically implanted pressure sensors: challenges and state of the field," Sensors, vol. 14, no. 11, pp. 20 620–20 644, 2014.

[28]. Harding C, Horsburgh B, Dorkin T, and Thorpe A, "Quantifying the Effect of Urodynamic Catheters on Urine Flow," Neurourol Urodyn., vol. 31, pp. 139–142, 2009.

[29]. Lutz BR, Venkataraman P, and Browd SR, "New and improved ways to treat hydrocephalus: Pursuit of a smart shunt." Surgical Neurology International, vol. 4, no. Suppl 1, pp. S38–50, 1 2013. [PubMed: 23653889]

[30]. Khoyratty SI, Gajendragadkar PR, Polisetty K, Ward S, Skinner T, and Gajendragadkar PR, "Flow rates through intravenous access devices: An in vitro study," Journal of Clinical Anesthesia, vol. 31, pp. 101–105, 2016. [PubMed: 27185686]
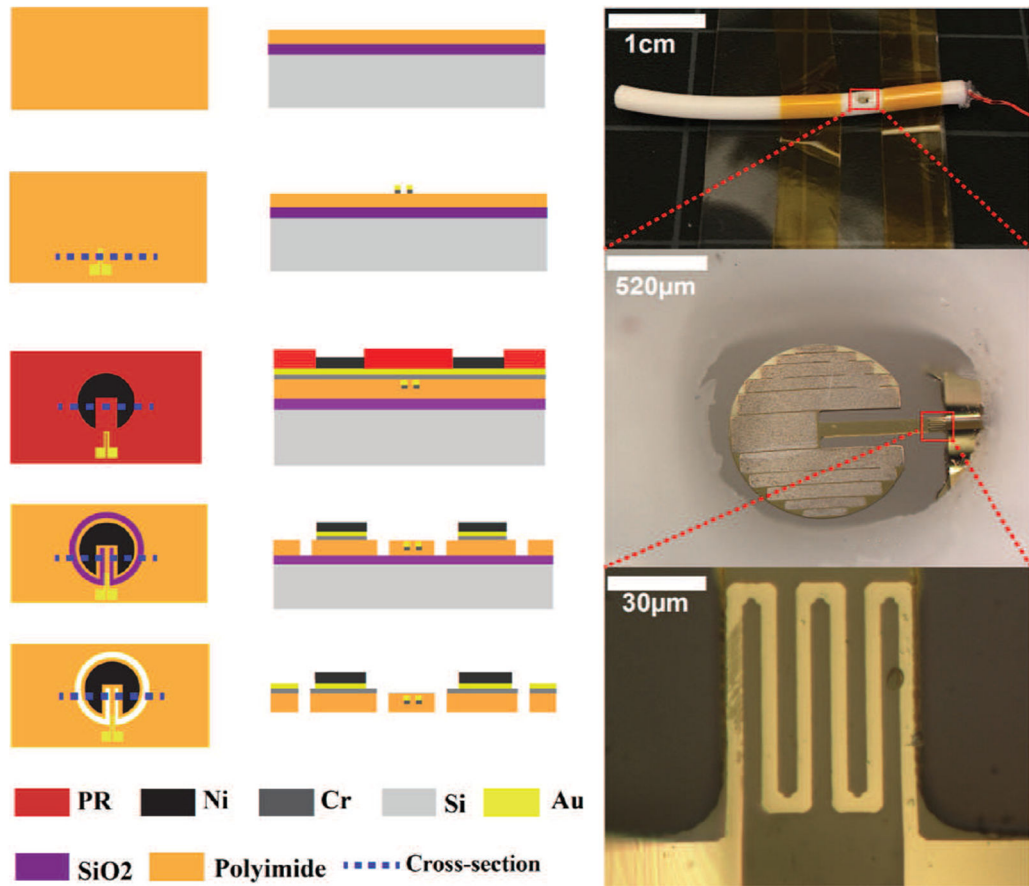
Fig. 1.
Process flow and fabricated multifunctional smart catheter. Left: top and corresponding cross-sectional views of each fabrication step. Right: photographs of fully integrated smart catheter with piezoresistor-embedded multifunctional magnetic microactuators.
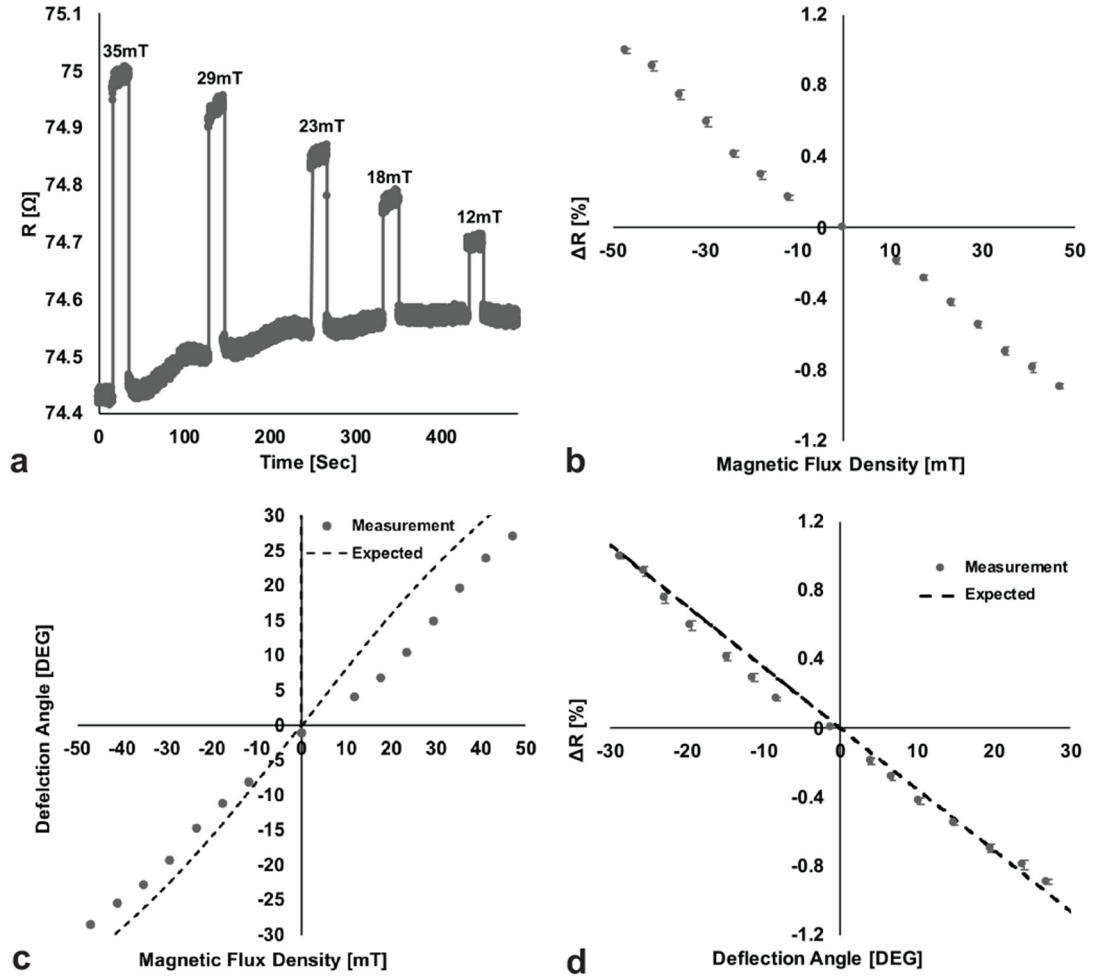
Fig. 2.
Static characterization. (a) Resistance value under various pulsed magnetic flux density. (b) Percentage of resistance change as a function of actuation strength and actuation direction. Positive change indicates deflecting downwards and negative change indicates deflecting upwards (n = 3). (c) Deflection angle as a function of magnetic flux density (n = 3). Theoretical line calculated by torque balance (Eq. 3). (d) Percentage of resistance change as a function of deflection angle (n = 3). Theoretic line indicates predicted value of resistance change of $G = 1.1$ for sample with $L = 655\mu$m, $w = 76\mu$m, $t = 12\mu$m)
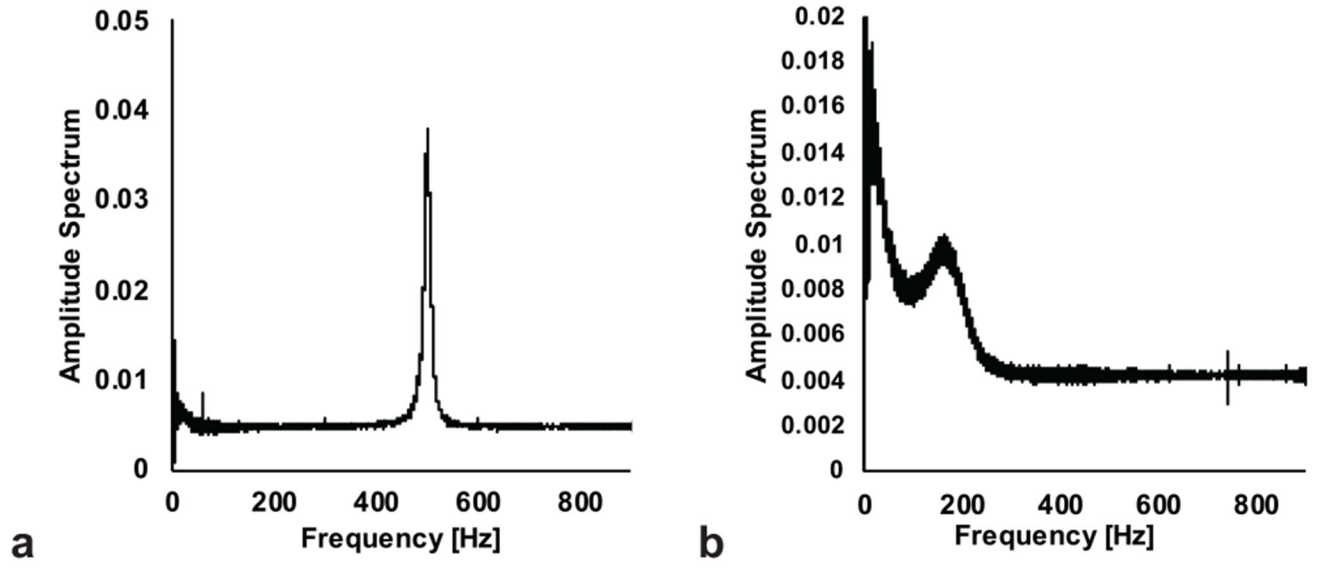
Fig. 3.
Dynamic characterization. Representative frequency responses from the integrated strain gauge in a smart catheter (a) in air and (b) DI water.
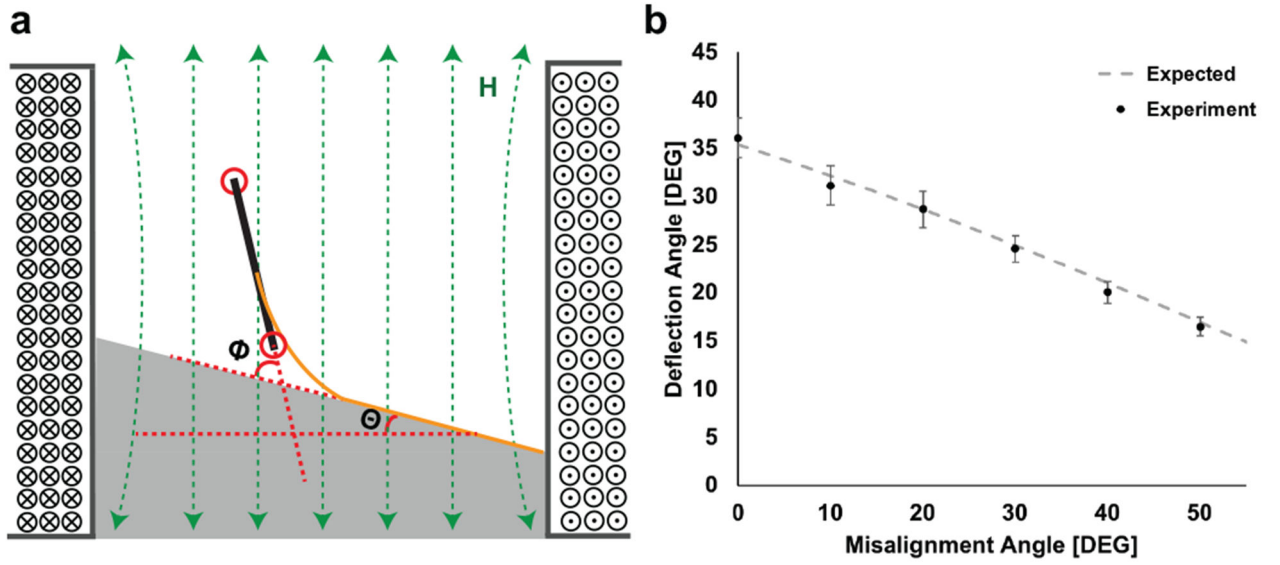
Fig. 4.
(a) Illustration of device misalignment. If the device orientation is not perpendicular to the applied magnetic field, the misalignment angle θ can affect the device deflection φ. (b) Deflection angle as a function of misalignment. For a given magnetic field strength, the deflection angle φ decreases as a function of misalignment θ which can be used to ensure that the magnet is oriented properly during actuation (n = 3). Theoretical line calculated for sample with $v_m = 0.003$ mm^3, $L = 405$ μm, $t = 12$ μm and $w = 47.5$ μm
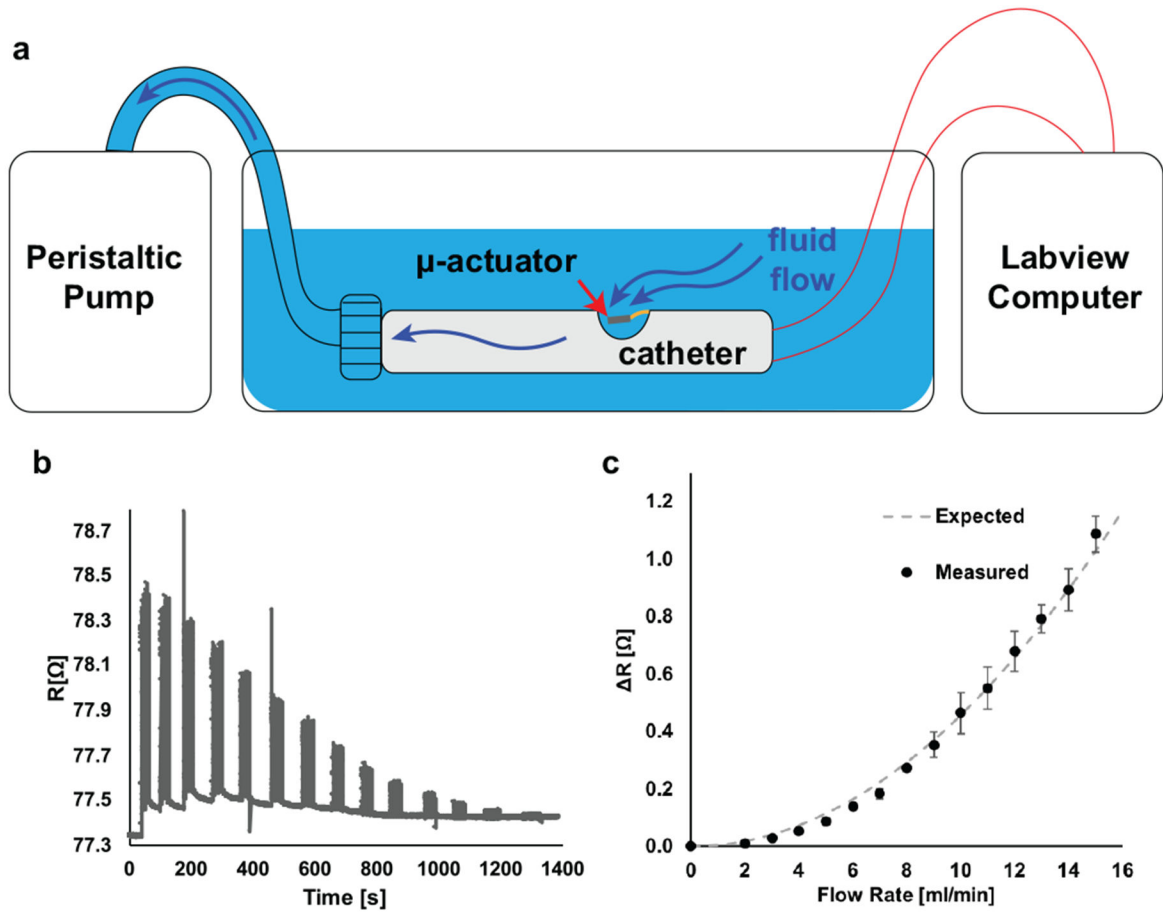
Fig. 5.
(a) Schematic of flow rate measurement. The peristaltic pump draws the fluid into the
catheter which deflects the microactuator. The strain gauge on the microactuators can be
used to calculate the flow rate. (b) Example of continuous measurement of piezoresistor
response at various flow rates. (c) Change in resistance as a function of flow rate. Note that
the expected values were calculated using $G = 1.1$ and drag coefficient $C_d = 2$ (n = 3) for
sample with $L = 655$ μm, $w = 76$ μm, $t = 12$ μm. Flow velocity v is calculated from flow rate
(2-15 ml/min) through the catheter with inner diameter ID of 0.9144 mm. Structural plate
area A is calculated from circle with diameter of 850 μm. Water density $\rho = 1000$ Kg/m^3 is
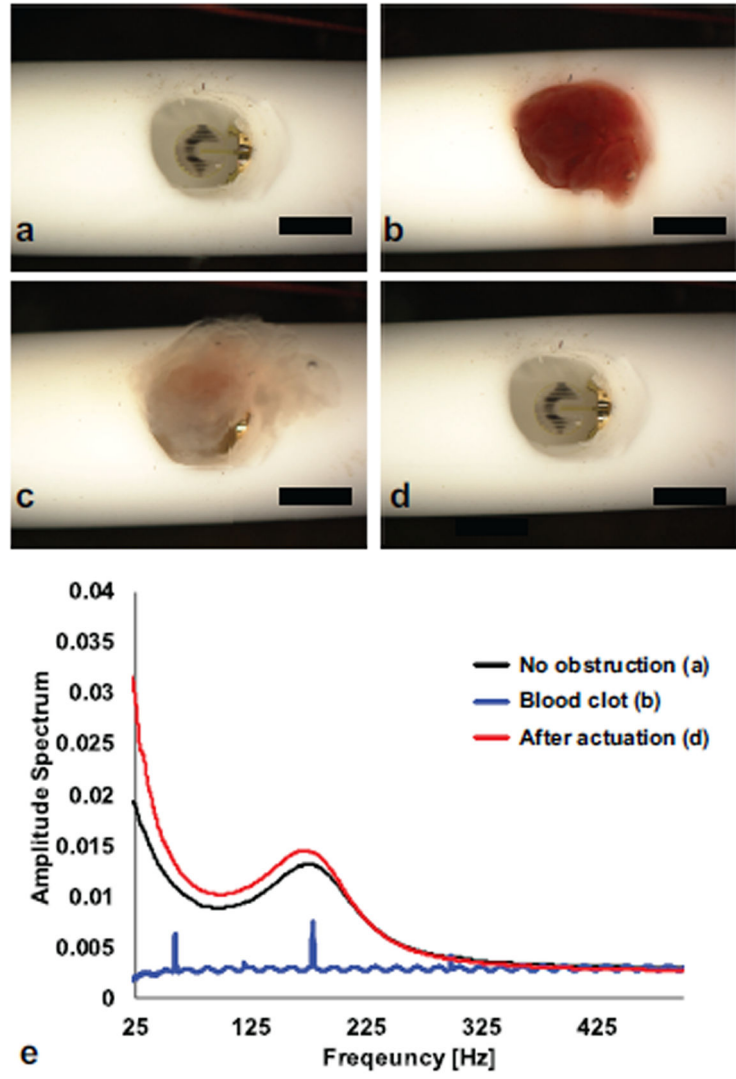used.

Fig. 6.

Optical images of catheter pore before and after blood clot obstruction removal: (a) before blood clot occlusion, (b) occluded catheter pore, (c) during actuation, and (d) after the blood clot removal. (scale bar = 1 mm) (e) Corresponding frequency responses before and after blood clot obstruction. Note that when the blood clot is obstructing the inlet pore, the dynamic response is completely attenuated. Following large amplitude actuation and blood clot removal, the dynamic response is restored to show characteristic peaks.